

RSC Advances



This is an *Accepted Manuscript*, which has been through the Royal Society of Chemistry peer review process and has been accepted for publication.

Accepted Manuscripts are published online shortly after acceptance, before technical editing, formatting and proof reading. Using this free service, authors can make their results available to the community, in citable form, before we publish the edited article. This *Accepted Manuscript* will be replaced by the edited, formatted and paginated article as soon as this is available.

You can find more information about *Accepted Manuscripts* in the [Information for Authors](#).

Please note that technical editing may introduce minor changes to the text and/or graphics, which may alter content. The journal's standard [Terms & Conditions](#) and the [Ethical guidelines](#) still apply. In no event shall the Royal Society of Chemistry be held responsible for any errors or omissions in this *Accepted Manuscript* or any consequences arising from the use of any information it contains.

Cite this: DOI: 10.1039/xxxxxxxxxx

Hybrid structures of BN nanoribbon/single-walled carbon nanotube: ab initio study†

Ping Lou *

Received Date
Accepted Date

DOI: 10.1039/xxxxxxxxxx

www.rsc.org/journalname

Hybrid structures of zigzag edge BN nanoribbon/single-walled carbon nanotube, namely, (i) ZBNNR-B-SWCNT in which only B-edge of zigzag edge BN nanoribbon (ZBNNR) is passivated with a single-walled carbon nanotube (SWCNT); (ii) ZBNNR-N-SWCNTs in which only N-edge of ZBNNR is terminated with a SWCNT; (iii) hydrogenated ZBNNR-B-SWCNT; (iv) hydrogenated ZBNNR-N-SWCNT, have been studied via standard spin-polarized density functional theory (DFT) calculations as well as ab initio molecular dynamics (MD) simulations. The DFT calculations and ab initio MD simulations results clearly show that all examined hybrid structures are stable at room temperature. Formation energy, as well as local DOS and Mulliken charge analysis, reveals that hybrid structure of ZBNNR-B-SWCNT is more stable than that of ZBNNR-N-SWCNT, since the covalent band of B-C is more strong than that of N-C owing to that the electronegativity difference of the N and C atoms (1.49) is larger than that of the C and B atoms (0.51). Surprisingly, the ZBNNR-B-SWCNTs belong to the intrinsic ferromagnetic metals, whereas the ZBNNR-N-SWCNTs belong to the intrinsic spin-gapless semiconductors (SGS). Furthermore, in contrast to hydrogenated ZBNNRs, which are nonmagnetic semiconductors, hydrogenated ZBNNR-N-SWCNTs turn into intrinsic spin-semiconductors (hydrogenation induces a SGS-spin-semiconductor transition), whereas hydrogenated ZBNNR-B-SWCNTs remain in the ferromagnetic metallic state, because H-passivation removes the dangling bond states of N-edge or B-edge, but the magnetic properties of "–SWCNT" edge remain unchanged.

1 Introduction

It is known that the graphene nanoribbons (GNRs) are made by cutting the graphene sheets, which edge carbon atoms are modified by hydrogen. Notably, the properties of GNRs are sensitive to the crystallographic orientation of the edges, with armchair type nanoribbons (AGNRs) belong to the nonmagnetic semiconductors. In contrast, GNRs having zigzag edges (ZGNRs) predicted to be the magnetic semiconductors with magnetically ordered edge states, which each edge is ferromagnetic order whereas between edges belong to antiferromagnetic coupling.¹ Theoretical studies revealed that such magnetically ordered edge state has a potential application in spintronics.^{2–5} Moreover, if the edges are not

straight, the edge magnetic coupling can be a ferromagnetic coupling.^{6,7} In addition, owing to the edge's chemical activity,^{8–10} different electronic and magnetic behaviors can be obtained when the two edges are terminated and passivated with different atoms or chemical groups.^{11–16}

In recent years, BN nanoribbons (BNNRs) have also attracted increasing attention.^{17–38} Experimental and theoretical studies have confirmed that the pristine BNNRs are magnetic metals.^{17,18} In pristine zigzag edge BNNRs with n chains (n -ZBNNRs), the two edges are respectively terminated by B and N atoms, namely one edge is terminated with B atoms (called as the N-edge), whereas another edge is terminated with N atoms (called as the B-edge, see Fig. 8(a)). Interestingly, when the B-edge is passivated with H atoms, it turns into a half-metallicity.^{19–21} In contrast, hydrogenated n -ZBNNR, as well as hydrogenated armchair edge BNNR with n dimer lines, belongs to a nonmagnetic semiconductor.^{22–24} Moreover, a lot of studies revealed that different electronic and magnetic behaviors can be obtained by various strategies, such as chemical functionalization,^{25–28} creating defects, impurity or doping,^{29–35} hydrogenation,³⁶ applying an external strain,³⁷ and applying an external electric fields.^{22,38}

On the other hand, a lot of studies revealed that the hy-

* Department of Physics, Anhui University, Hefei 230039, Anhui, China. Fax: +86-551-65107999; Tel: +86-551-65106477; E-mail: loup@ahu.edu.cn

† Electronic Supplementary Information (ESI) available: Supporting Fig.1 showing the band structure of 2ZBNNR-N-(4,4)SWCNT calculated with PBE functional and HSE06 hybrid functional, Supporting Fig.2 showing the relative energies for 2ZBNNR-N-(6,6)SWCNT in FM, AFM, and NM states, Supporting Fig.3 showing the relative energies for H-2ZBNNR-N-(6,6)SWCNT in FM, AFM, and NM states, Supporting Fig.4 showing the relative energies for 3ZBNNR-B-(6,6)SWCNT in FM, AFM, and NM states, and Supporting Fig.5 showing the relative energies for H-3ZBNNR-B-(6,6)SWCNT in FM and NM states. See DOI: 10.1039/b000000x/

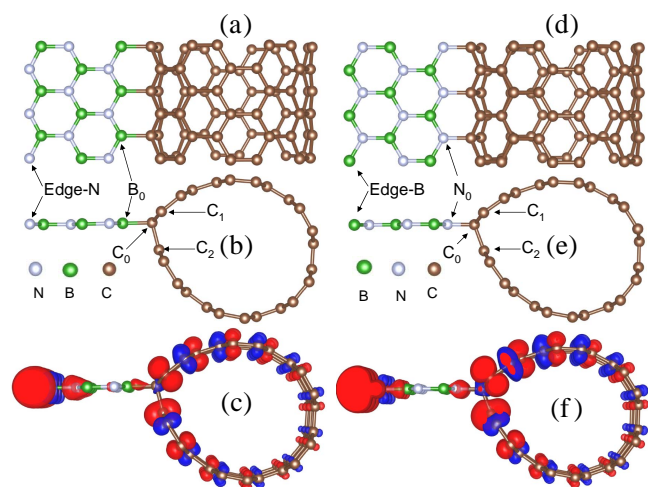


Fig. 1 (a) Top view and (b) side view of 3ZBNRR-B-(6,6)SWCNT, and (c) is spatial distribution of the spin differences. (d) Top view and (e) side view of a 3ZBNRR-N-(6,6)SWCNT, and (f) is spatial distribution of the spin differences. C_0 , C_1 , and C_2 mark the special C sites. Edge-B and B_0 mark the special B sites, whereas edge-N and N_0 mark the special N sites. The red and blue surfaces represent the spin-up (\uparrow) and spin-down (\downarrow). The isosurface of $0.003 \mu_B/\text{\AA}^3$ is adopted for the spin-up (\uparrow), whereas the isosurface of $0.0015 \mu_B/\text{\AA}^3$ is adopted for the spin-down (\downarrow).

brid structures of BNNR/GNR also show rich electronic and magnetic properties,^{39–48} such as the band gap and edge magnetism of the hybrid BN-C nanoribbons can be regulated by the BN/C ratio.⁴⁵ Recently, Du et al. have studied the hybrid C-BN single-walled nanotubes and found that zigzag $C_{0.5}(\text{BN})_{0.5}$ SWNTs belong to narrow gap semiconductors, whereas armchair $C_{0.5}(\text{BN})_{0.5}$ SWNTs belong to gapless semiconductors.⁴⁸

Furthermore, there has been increasing evidence that d and f metal elements are not the sole source in inducing intrinsic magnetism. It is known that metal-free ferromagnetism holds great promise to overcome the limitations of technologies relying on current magnetic materials based on d and f metal elements as they involve only 2p elements. Moreover, owing to the 2p electron systems with weak spin-orbit coupling and a relatively long spin relaxation time, the metal-free ferromagnetism would play an important role in constructing future-generation spintronic devices.^{49,50} It is hence highly desirable to design and develop ferromagnetism materials based on 2p elements instead of d and f metal elements.

Herein, hybrid structures of n -ZBNRR/ (m,m) SWCNT, namely, (i) pristine n ZBNRR-B- (m,m) SWCNTs in which the B-edge of pristine ZBNRR is passivated with a (m,m) SWCNT (see Fig. 1(a)-(b)); (ii) pristine n ZBNRR-N- (m,m) SWCNTs in which the N-edge of pristine ZBNRR is passivated with a (m,m) SWCNT (see Figure 1(d)-(e)); (iii) hydrogenated n ZBNRR-N- (m,m) SWCNTs (H- n ZBNRR-N- (m,m) SWCNTs, see Fig. 3(a)); (iv) hydrogenated n ZBNRR-B- (m,m) SWCNTs (H- n ZBNRR-B- (m,m) SWCNTs, see Fig. 3(b)), were studied via standard spin-polarized density functional theory (DFT) calculations as well as ab initio

molecular dynamics (MD) simulations. The DFT calculations and ab initio MD simulations results clearly show that all examined hybrid structures are stable at room temperature. Formation energy, local DOS, and Mulliken charge analysis reveal that hybrid structure of ZBNRR-B-SWCNT is more stable than that of ZBNRR-B-SWCNT. Fascinatingly, we find that pristine n ZBNRR-B- (m,m) SWCNTs belong to the intrinsic ferromagnetic metals, whereas pristine n ZBNRR-N- (m,m) SWCNTs belong to the intrinsic spin-gapless semiconductors.^{51,52} Moreover, hydrogenation makes the n ZBNRR-N- (m,m) SWCNTs become the ferromagnetic intrinsic spin-semiconductors,^{53–55} whereas hydrogenated n ZBNRR-B- (m,m) SWCNTs remain the intrinsic ferromagnetic metals. They are viewed as one of the most ideal materials for constructing metal-free spintronic nanodevices.^{51–54}

2 Computational methods

All full structural optimizations, total energy, and electronic structure calculations are performed in the framework of spin-polarized density functional theory (DFT), as implemented in the numerical atomic orbitals basis-set OPENMX computer code.⁵⁶ The DFT within the generalized gradient approximation (GGA)⁵⁷ for the exchange-correlation energy was adopted. Norm-conserving Kleinman-Bylander pseudopotentials⁵⁸ were employed, and the wave functions were expanded by a linear combination of multiple pseudo atomic orbitals (LCPAO)^{59,60} with a kinetic energy cutoff of 300 Ry. The basis functions used were B7.0- $s^2p^1d^1$, C7.0- $s^2p^2d^1$, N7.0- $s^2p^3d^1$, and H7.0- s^1p^1 . The first symbol designates the chemical name, followed by the cutoff radius (in Bohr radius) in the confinement scheme and the last set of symbols defines the primitive orbitals applied. We adopted a supercell geometry where the length of a vacuum region along the non-periodic direction (x -, y -directions) was 30 Å, and the lattice constant along the periodic direction (z -direction). $1 \times 1 \times 121$ k -point sampling points in the Brillouin zone integration was performed for reliable results.^{61–64} Structural optimizations were performed using the conjugate gradient algorithm until the residual forces were smaller than 10^{-4} Hartree/bohr. The convergence in energy was 10^{-8} Hartree. We have also increased the size of the supercell to make sure that it does not produce any discernible difference on the results.

On the other hand, ab initio MD simulations were performed by the canonical (NVT) ensemble and carried out with the OPENMX computer code,⁵⁶ in which the heat bath is realized by means of Nose-Hoover^{65,66} and the temperature is fixed at 298 K, the time step is 1.0 femtosecond, and the total steps are 10000.

3 Results and Discussion

3.1 Atomic geometries, electronic and magnetic properties

3.1.1 Atomic geometries and spin distribution

Fig. 1 plots the atomic geometries and spatial distribution of the spin differences for 3ZBNRR-B-(6,6)SWCNT and 3ZBNRR-N-(6,6)SWCNT, respectively. From Fig. 1(a)-(b), one can find that in 3ZBNRR-B-(6,6)SWCNT, via the bonding of C_0 and B_0 atoms, the pristine n -ZBNRR and pristine (6,6)SWCNT bonded with each other. From Fig. 1(d)-(e), one can find that in 3ZBNRR-

Table 1 The magnetic moments on each C_0 , C_1 , C_2 , B_0 , and edge-N atom, and in a unite cell, in the unit of μ_B for pristine and hydrogenation n ZBNNR-B-(6,6)SWNT ($n=3$ and 6).

n ZBNNR-B-(6,6)SWNT	C_0	C_1	C_2	B_0	edge-N	Cell
Pristine						
3	-0.02	0.18	0.18	0.02	0.79	1.4
6	-0.02	0.21	0.09	0.02	0.88	1.4
Hydrogenation						
3	-0.03	0.23	0.07	0.02	0.00	0.5
6	-0.03	0.25	0.09	0.03	0.00	0.6

Table 2 The magnetic moments on each C_0 , C_1 , C_2 , N_0 , and edge-B atom, and in a unite cell, in the unit of μ_B for pristine and hydrogenation n ZBNNR-N-(6,6)SWNT ($n=3$ and 6).

n ZBNNR-N-(6,6)SWNT	C_0	C_1	C_2	N_0	edge-B	Cell
Pristine						
3	-0.06	0.41	0.32	0.04	0.98	1.9
6	-0.06	0.42	0.33	0.04	1.00	2.0
Hydrogenation						
3	-0.06	0.42	0.35	0.05	0.00	1.0
6	-0.06	0.42	0.35	0.05	0.00	1.0

N-(6,6)SWCNT, via the bonding of C_0 and N_0 atoms, the pristine n -ZBNNR and pristine (6,6)SWCNT bonded with each other. Note that each C_0 atom has four nearest neighbor atoms and is sp^3 -hybridized. As a result, in 3ZBNNR-B-(6,6)SWCNT, the each C_0 and four nearest neighbor atoms form one C-B bond and three C-C bonds (C_0 -B, C_0 - C_2 , and two C_0 - C_1 bonds), whereas in 3ZBNNR-N-(6,6)SWCNT, the each C_0 and four nearest neighbor atoms form one C-N bond and three C-C bonds (C_0 -N, C_0 - C_2 , and two C_0 - C_1 bonds). Clearly, both 3ZBNNR-B-(6,6)SWCNT and 3ZBNNR-N-(6,6)SWCNT possess the sp^3 -hybridized Y-shape and remaining tube-shape stability structures commonly used for building construction. As a result, 3ZBNNR-B-(6,6)SWCNT, as well as 3ZBNNR-N-(6,6)SWCNT, entails much greater flexural rigidity than a 3-ZBNNR. In addition, in Table 1, we have listed the magnetic moments on each C_0 , C_1 , C_2 , B_0 , and edge-N atom, as well as per unite cell, for 3ZBNNR-B-(6,6)SWNTs, whereas Table 2 show the magnetic moments on each C_0 , C_1 , C_2 , N_0 and edge-B atom, as well as per unite cell, for 3ZBNNR-N-(6,6)SWNT. As shown in Table 1, each C_1 , C_2 , and edge-N atom possesses relatively large magnetic moments with same spin orientation. As a result, 3ZBNNR-B-(6,6)SWCNT has a ferromagnetic ground state with net magnetic moment of $1.4 \mu_B$ per unit cell. As shown in Table 2, each C_1 , C_2 , and edge-B atom possesses relatively large magnetic moments with same spin orientation. As a result, 3ZBNNR-N-(6,6)SWCNT possesses a ferromagnetic ground state with net magnetic moment of $1.9 \mu_B$ per unit cell.

3.1.2 Band structures

The spin-polarized band structures for pristine 6ZBNNR-N-(6,6)SWCNT and 6ZBNNR-B-(6,6)SWCNT (respectively named as 6ZBNNR-N-(6,6)SWCNT and 6ZBNNR-B-(6,6)SWCNT) are shown in Fig. 2 (the relative stability of the ferromagnetic, antiferromagnetic, and nonmagnetic states is shown in ESI Fig. 2† and Fig. 4†). Clearly, from Fig. 2(a), one can find that in the band structure of 6ZBNNR-N-(6,6)SWCNT, both spin channels are gapped, but the spin-down conduction band minimum and

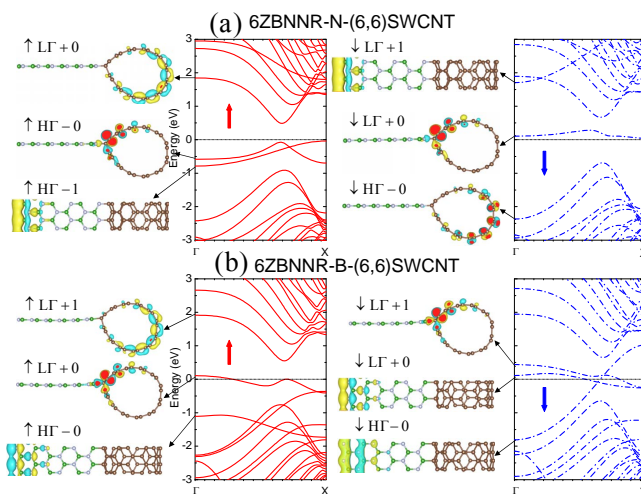


Fig. 2 Spin-polarized band structures and partial charge densities of the unoccupied band (L Γ) and the occupied band (H Γ) at the Γ point. (a) Pristine 6ZBNNR-N-(6,6)SWCNT. (b) Pristine 6ZBNNR-B-(6,6)SWCNT. The red solid and blue dash dotted lines denote the spin-up (\uparrow) and spin-down (\downarrow) bands, respectively. The Fermi level is set to zero. The isosurface is $0.05 e/\text{\AA}^3$.

the spin-up valence band maximum touch at the Fermi energy, i.e., "spin-gapless". Thus, 6ZBNNR-N-(6,6)SWCNT belongs to a intrinsic spin-gapless semiconductor (SGS), in which not only the excited electrons but also the holes can be fully spin polarized.⁵¹ On the other hand, in order to reveal the origin of its electronic band structure, we marked the energy bands near Fermi level via partial charge densities of the unoccupied band (L Γ) and the occupied band (H Γ) at the Γ point. From Fig. 2(a), one can find that the energy bands marked with \uparrow H Γ -0 and \downarrow L Γ +0 are contributed mainly by the atom orbitals of "(6,6)SWCNT" which is absent in 6-ZBNNR-NH, whereas the energy band marked with \uparrow H Γ -1 is contributed mainly by the atom orbitals of B-edge, which corresponds to the dangling-bond state. Thus, we can conclude that the unique electronic and magnetic properties of 6ZBNNR-N-(6,6)SWCNT are ascribable to the zigzag edge state of "6ZBNNR-N-" as well as the special edge shape of "(m,m)SWCNT". However, as shown in Fig. 2(b), 6ZBNNR-B-(6,6)SWCNT is a intrinsic ferromagnetic metal, owing to four bands crossing the Fermi level. On the other hand, the energy bands marked with \uparrow L Γ +0 and \downarrow L Γ +1 are contributed mainly by the atom orbitals of "(6,6)SWCNT" which is absent in 6-ZBNNR-BH, whereas the energy bands marked with \downarrow L Γ +0 and \downarrow H Γ -0 are contributed mainly by the atom orbitals of N-edge, which correspond to the dangling-bond state. Thus, we can conclude that the unique electronic and magnetic properties of 6ZBNNR-B-(6,6)SWCNT are ascribable to the zigzag edge state of "6ZBNNR-B-" as well as the special edge shape of "(m,m)SWCNT".

3.1.3 Hydrogenation effects

The spin-polarized band structures and spatial distribution of the spin differences for hydrogenated 6ZBNNR-B-(6,6)SWCNT and

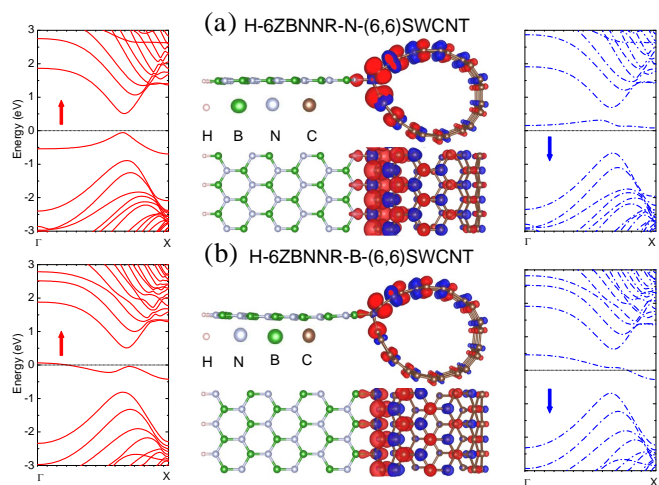


Fig. 3 Spin-polarized band structures and spatial distribution of the spin differences. (a) H-6ZBNNR-N-(6,6)SWCNT. (b) H-6ZBNNR-B-(6,6)SWCNT. The other marks are same as in Fig. 1 and Fig. 2.

6ZBNNR-N-(6,6)SWCNT (hereafter referred to as H-6ZBNNR-B-(6,6)SWCNT, H-6ZBNNR-N-(6,6)SWCNT) are shown in Fig. 3 (the relative stability of the ferromagnetic, antiferromagnetic, and nonmagnetic states is shown in ESI Fig. 3† and Fig. 5†). Clearly, as shown in Fig. 3(b), the H-6ZBNNR-B-(6,6)SWCNT belongs to an intrinsic ferromagnetic metal,⁵⁵ which is ascribable to the energy bands marked with $\uparrow\text{L}\Gamma+0$ and $\downarrow\text{L}\Gamma+1$ shown in Fig. 2(b). Comparing between Fig. 2(b) and Fig. 3(b), one can find that the $\downarrow\text{L}\Gamma+0$ band that appears in 6ZBNNR-B-(6,6)SWCNT disappears in the H-6ZBNNR-B-(6,6)SWCNT, which indicates that the dangling-bond state of the N-edge is removed by H-passivation. Meanwhile, the local spin moment on each edge-N atom vanishes. As a result, the H-6ZBNNR-B-(6,6)SWCNT has a net magnetic moment of $0.6 \mu_{\text{B}}$ per unit cell (see Table 1). Thus, we can conclude that the unique electronic and magnetic properties of the H-6ZBNNR-B-(6,6)SWCNT are ascribable to the special edge shape of " $-(m,m)$ SWCNT". In contrast, the H-6ZBNNR-N-(6,6)SWCNT becomes an intrinsic spin-semiconductor,^{53,55} in which completely spin-polarized currents can be created and manipulated only just by applying a gate voltage. On the other hand, comparing between Fig. 3(a) and Fig. 2(a), one can find that the $\uparrow\text{H}\Gamma-1$ band that appears in 6ZBNNR-N-(6,6)SWCNT disappears in H-6ZBNNR-N-(6,6)SWCNT and a spin band gap opens, namely hydrogenation induces a SGS-spin-semiconductor transition. This is because H-passivation removes the dangling-bond state of the B-edge. Meanwhile, the local spin moment on each edge-B atom vanishes. As a result, the H-6ZBNNR-N-(6,6)SWCNT has a net magnetic moment of $1.0 \mu_{\text{B}}$ per unit cell (see Table 2). Thus, we can conclude that the unique electronic and magnetic properties of the H-6ZBNNR-N-(6,6)SWCNT originate from the special edge shape of " $-(m,m)$ SWCNT".

Comparing between results of the pristine and hydrogenated hybrid structures of ZBNNR/SWCNT, we can conclude that the

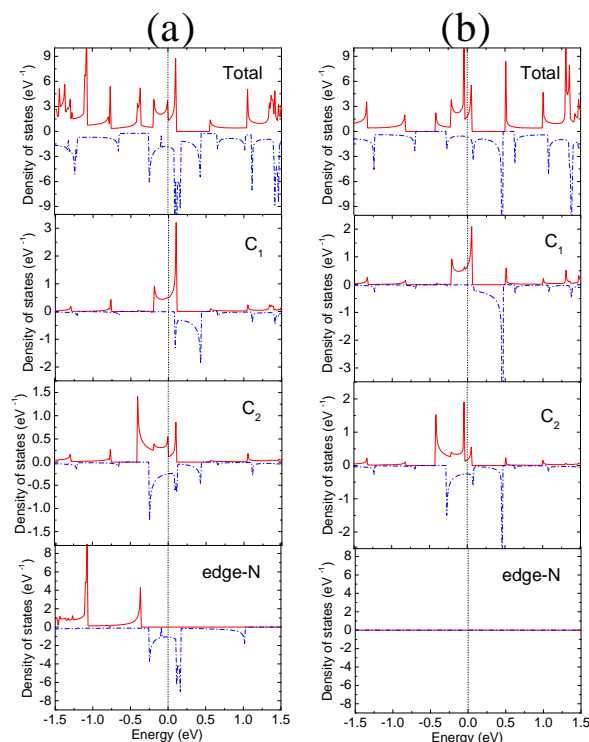


Fig. 4 Total density of states (TDOS) and local DOS (LDOS). (a) 6ZBNNR-B-(6,6)SWCNT. (b) H-6ZBNNR-B-(6,6)SWCNT. The other marks are same as in Fig. 2.

unique electronic and magnetic properties of the pristine hybrid structures originate from the zigzag edge state of " n ZBNNR-B-" (" n ZBNNR-N-") and the special edge shape of " $-(m,m)$ SWCNT". However, the unique electronic and magnetic properties of the hydrogenated hybrid structures only are ascribable to the special edge shape of " $-(m,m)$ SWCNT".

3.1.4 Analysis of density of states

The above results can be further understood by the analysis of the total density of states (TDOS) and the local density of states (LDOS). Fig. 4(a) and Fig. 4(b) plot the TDOS and LDOS for 6ZBNNR-B-(6,6)SWCNT and H-6ZBNNR-B-(6,6)SWCNT, respectively. From Fig. 4(a), one can find that in 6ZBNNR-B-(6,6)SWCNT, the TDOS near the Fermi level are contributed not only by the C_1 and C_2 atoms of " $-(6,6)$ SWCNT", but also by the edge-N atom of "6ZBNNR". However, as shown in Fig. 4(b), in H-6ZBNNR-B-(6,6)SWCNT, hydrogenation removes the contribution of the edge-N atom of "6ZBNNR" completely. On the other hand, as shown in Fig. 4(a), before hydrogenation, in 6ZBNNR-B-(6,6)SWCNT, for the edge-N, C_1 and C_2 atoms, the peak of LDOS in the spin-up channel is below the Fermi level, while the peak of LDOS in the spin-down channel is above the Fermi level. As a result, the edge-N, C_1 and C_2 atoms possess spin-up local magnetic moment. However, as shown in Fig. 4(b), after hydrogenation, in H-6ZBNNR-B-(6,6)SWCNT, the peaks of LDOS of C_1 and C_2 atoms remain unchanged, but the peak of LDOS of the edge-N atom disappears completely. As a result, C_1 and C_2 atoms remain

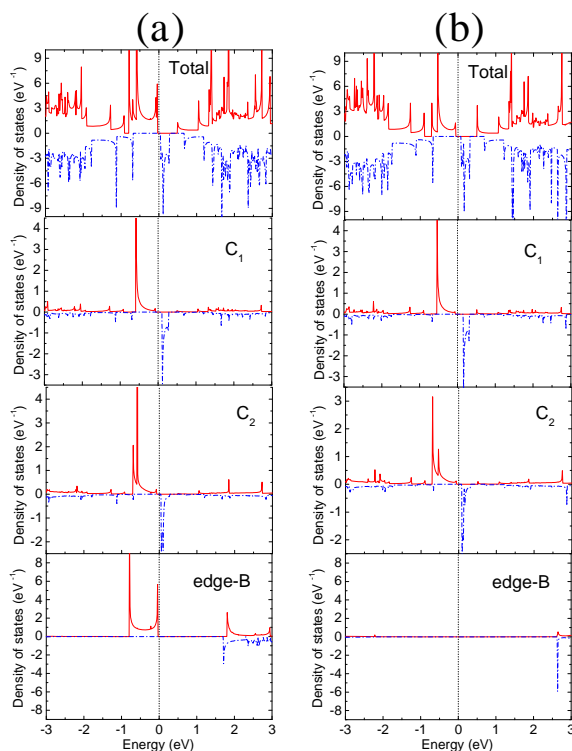


Fig. 5 TDOS and LDOS. (a) 6ZBNNR-N-(6,6)SWCNT. (b) H-6ZBNNR-N-(6,6)SWCNT. The other marks are same as in Fig. 2.

to possess spin-up local magnetic moment, whereas, the local magnetic moment on the edge-N atom has been removed completely. In addition, from Fig. 4(a), one can find that in 6ZBNNR-B-(6,6)SWCNT, the LDOS in the spin-up channel of the C_1 atom crosses the Fermi level, the LDOSs in the spin-up and spin-down channels of the C_1 atoms cross the Fermi level, whereas the LDOS in the spin-down channel of the edge-N atom crosses the Fermi level, which indicate that the orbitals of the edge-N, C_1 and C_2 atoms take part in electric conduction, namely, N edge and "-(6,6)SWCNT" edge undertake electric conduction responsibility. However, as shown in Fig. 4(a), one can find that after hydrogenation, in H-6ZBNNR-B-(6,6)SWCNT, the orbital of the edge-N atom is no longer taking part in the electric conduction process, namely, only "-(6,6)SWCNT" edge undertakes electric conduction responsibility. It is worth mentioning that because the electrically conductive function and magnetic properties of 6-ZBNNR are undertaken by the dangling-bond states at its B-edge and N-edge, hydrogenation makes it become nonmagnetic semiconductor^{19–21} owing to the dangling-bond states to have been removed by H-passivation. However, in H-6ZBNNR-B-(6,6)SWCNT, H-passivation removes the dangling-bond states at its N-edge, but the electrically conductive function and magnetic properties of "-(6,6)SWCNT" edge is retained.

The TDOS and LDOS for 6ZBNNR-N-(6,6)SWCNT and H-6ZBNNR-N-(6,6)SWCNT are plotted in Fig. 5(a) and Fig. 5(b), respectively. From Fig. 5(a), one can find that in 6ZBNNR-N-(6,6)SWCNT, the TDOS near Fermi level are contributed not only

by the C_1 and C_2 atoms of "-(6,6)SWCNT", but also by the edge-B atom of "6ZBNNR". However, as shown in Fig. 5(b), in H-6ZBNNR-N-(6,6)SWCNT, hydrogenation removes the contribution of the edge-B atom of 6ZBNNR completely. Moreover, as shown in Fig. 5(a), in 6ZBNNR-N-(6,6)SWCNT, for the edge-B, C_1 and C_2 atoms, the peak of LDOS in the spin-up channel is below the Fermi level, while the peak of LDOS in the spin-down channel is above the Fermi level. As a result, the edge-B, C_1 and C_2 atoms possess spin-up local magnetic moment. However, as shown in Fig. 5(b), in H-6ZBNNR-N-(6,6)SWCNT, namely after hydrogenation, below the Fermi level, the the peak of LDOS of the edge-B atom disappears completely, but the peaks of LDOS of C_1 and C_2 atoms remain unchanged. As a result, the local magnetic moment on the edge-B atom is removed completely, whereas, the spin-up local magnetic moments on C_1 and C_2 atoms remain unchanged. On the other hand, that the peak of LDOS of the edge-B atom disappears leads to a band gap between the spin-up and spin-down channels. As a result, the H-6ZBNNR-N-(6,6)SWCNT is a intrinsic spin-semiconductor,⁵³ in which hydrogenation induces a SGS-spin-semiconductor transition.

3.1.5 Mulliken charge and spin population analysis

In order to further understand the above results, we calculate the Mulliken charge and spin population of the special atoms. For example, the Mulliken charge and spin population on each C_0 , C_1 , C_2 , B_0 , and edge-N atom for pristine and hydrogenation 6ZBNNR-B-(6,6)SWNT are listed in Table 3. As shown in Table 3, the local magnetic moment on each C_0 , C_1 , C_2 , B_0 , and edge-N atom originate from the difference between the spin-up and spin-down charges. Such as, in 6ZBNNR-B-(6,6)SWNT, the charges on each C_1 atom are 2.028 and 1.824 e for spin-up and spin-down channels, respectively. As a result, each C_1 atom possesses 0.204 μ_B spin-up local magnetic moment. After hydrogenation, namely in H-6ZBNNR-B-(6,6)SWNT, the charges on each C_1 atom are 2.057 and 1.807 e for spin-up and spin-down channels, respectively. As a result, each C_1 atom has 0.250 μ_B spin-up local magnetic moment. Most notably, after hydrogenation the charge and spin population of edge-N atom occurs significant change. As shown in Table 3, in 6ZBNNR-B-(6,6)SWNT, the charges on edge-N atom are 3.081 and 2.203 e for spin-up and spin-down channels, respectively. As a result, each edge-N atom possesses 0.878 μ_B spin-up local magnetic moment. After hydrogenation, namely in H-6ZBNNR-B-(6,6)SWNT, the charges on each edge-N atom are 2.823 and 2.823 e for spin-up and spin-down channels, respectively. As a result, the local magnetic moment on each edge-N atom is 0.000 μ_B , namely, the local magnetic moment on each edge-N atom has been removed.

Similarly, the Mulliken charge and spin population on each C_0 , C_1 , C_2 , N_0 , and edge-B atom for pristine and hydrogenation 6ZBNNR-N-(6,6)SWNT are listed in Table 4. As shown in Table 4, after hydrogenation, except the charge and spin population of edge-B atom, there is no significant change in the charge and spin population of system. Such as, before hydrogenation, namely in 6ZBNNR-N-(6,6)SWNT, the charges on each C_2 atom are 2.165 and 1.835 e for spin-up and spin-down channels, respectively. As a result, each C_2 atom has 0.330 μ_B spin-up local magnetic mo-

Table 3 The Mulliken charge and spin population on each C₀, C₁, C₂, B₀, and edge-N atom for pristine and hydrogenation 6ZBNNR-B-(6,6)SWNT.

System	spin-up	spin-down	sum	diff
6ZBNNR-B-(6,6)SWNT	1.996	C ₀ 2.018	4.014	-0.022
H-6ZBNNR-B-(6,6)SWNT	1.992	2.019	4.011	-0.027
6ZBNNR-B-(6,6)SWNT	2.028	C ₁ 1.824	3.852	0.204
H-6ZBNNR-B-(6,6)SWNT	2.057	1.807	3.864	0.250
6ZBNNR-B-(6,6)SWNT	2.059	C ₂ 1.973	4.032	0.086
H-6ZBNNR-B-(6,6)SWNT	2.063	1.974	4.037	0.089
6ZBNNR-B-(6,6)SWNT	1.388	B ₀ 1.366	2.754	0.022
H-6ZBNNR-B-(6,6)SWNT	1.390	1.365	2.755	0.025
6ZBNNR-B-(6,6)SWNT	3.081	edge-N 2.203	5.284	0.878
H-6ZBNNR-B-(6,6)SWNT	2.823	2.823	5.646	0.000

Table 4 The Mulliken charge and spin population on each C₀, C₁, C₂, N₀, and edge-B atom for pristine and hydrogenation 6ZBNNR-N-(6,6)SWNT.

System	spin-up	spin-down	sum	diff
6ZBNNR-N-(6,6)SWNT	1.832	C ₀ 1.889	3.721	-0.057
H-6ZBNNR-N-(6,6)SWNT	1.829	1.887	3.716	-0.058
6ZBNNR-N-(6,6)SWNT	2.175	C ₁ 1.757	3.932	0.418
H-6ZBNNR-N-(6,6)SWNT	2.176	1.756	3.932	0.420
6ZBNNR-N-(6,6)SWNT	2.165	C ₂ 1.835	4.000	0.330
H-6ZBNNR-N-(6,6)SWNT	2.172	1.827	3.999	0.345
6ZBNNR-N-(6,6)SWNT	2.802	N ₀ 2.759	5.561	0.043
H-6ZBNNR-N-(6,6)SWNT	2.804	2.759	5.563	0.045
6ZBNNR-N-(6,6)SWNT	1.893	edge-B 0.898	2.791	0.995
H-6ZBNNR-N-(6,6)SWNT	1.402	1.402	2.804	0.000

ment. After hydrogenation, namely in H-6ZBNNR-N-(6,6)SWNT, the charges on each C₂ atom are 2.172 and 1.827 *e* for spin-up and spin-down channels, respectively. As a result, each C₂ atom has 0.345 μ_B spin-up local magnetic moment. Most notably, after hydrogenation the charge and spin population of edge-B atom occurs significant change. As shown in Table 4, before hydrogenation, namely in 6ZBNNR-N-(6,6)SWNT, the charges of edge-B atom are 1.893 and 0.898 *e* for spin-up and spin-down channels, respectively. As a result, each edge-B atom has 0.995 μ_B spin-up local magnetic moment. After hydrogenation, namely in H-6ZBNNR-N-(6,6)SWNT, the charges on each edge-B atom are 1.402 and 1.402 *e* for spin-up and spin-down channels, respectively. As a result, the local magnetic moment on each edge-B atom is 0.000 μ_B, i.e., the local magnetic moment on each edge-B atom vanishes.

3.1.6 Origin of magnetism

The origin of magnetism in the hybrid structures of ZBNNR/SWCNT is related to its electronic structures. For example, the spin-unpolarized band structures of the 6ZBNNR-B-(6,6)SWCNT is shown in Fig. 6(a), whereas its corresponding the total density of states and the LDOS are shown in Fig. 7(a). From Fig. 6(a), one can find that there are three energy bands, marked with LG+0, HΓ-0, and HΓ-1 or LX+0, HX-0 as well as HX-1, crossing the Fermi level and are called as the partial-filled bands. Clearly, the partial charge densities of the

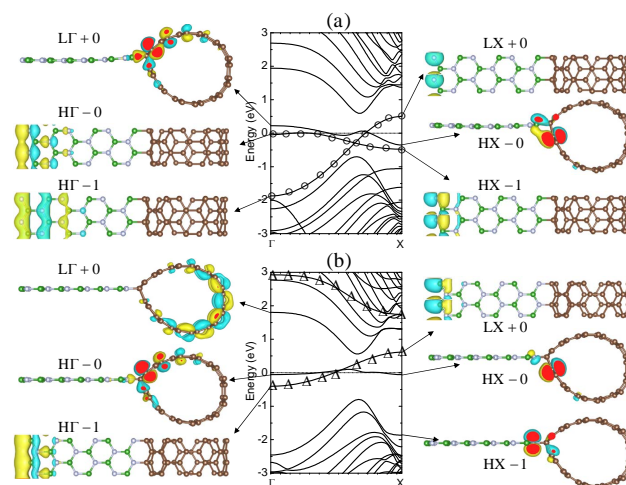
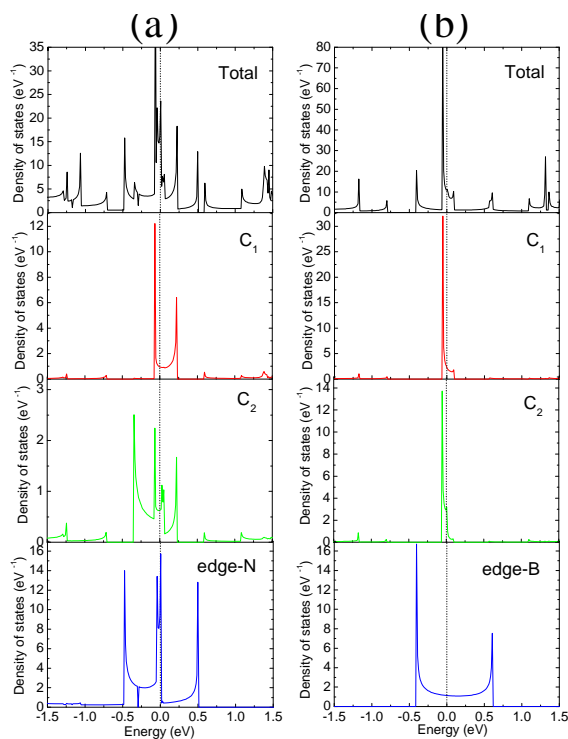


Fig. 6 Spin-unresolved band structures and partial charge densities of the unoccupied band (LG) and the occupied band (HΓ) at the Γ and X points. (a) 6ZBNNR-B-(6,6)SWCNT. (b) 6ZBNNR-N-(6,6)SWCNT. "o" and "△" label special bands (see Fig. 8). The other marks are same as in Fig. 2.

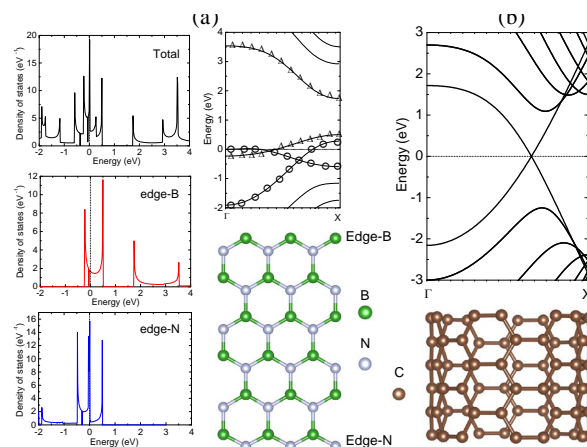
Table 5 The formation energy in the unit of eV for pristine n ZBNNR-B-(6,6)SWNT and n ZBNNR-N-(6,6)SWNT.

System	$n=3$	$n=4$	$n=5$	$n=6$	$n=7$	$n=8$
n ZBNNR-B-(6,6)SWNT	-2.28	-2.48	-2.51	-2.56	-2.58	-2.59
n ZBNNR-N-(6,6)SWNT	-1.80	-2.08	-2.15	-2.18	-2.21	-2.25

**Fig. 7** TDOS and LDOS. (a) 6ZBNNR-B-(6,6)SWCNT. (b) 6ZBNNR-N-(6,6)SWCNT. The other marks are same as in Fig. 2.

unoccupied band and the occupied band plotting in Fig. 6(a) show that the partial-filled bands corresponding electron states are heavily localized. Indeed, as shown in Fig. 7(a), the LDOS analysis reveal that they are strongly localized on the C_1 and C_2 atoms of “-(6,6)SWCNT” as well as the edge-N atom of “6ZBNNR”. According to Hund’s rule, such partial filling of the localized bands drives spontaneous spin polarization, resulting in exchange splittings between $\downarrow L\Gamma+0$ and $\uparrow L\Gamma+0$ bands, as well as between $\downarrow L\Gamma+0$ and $\uparrow H\Gamma-0$ bands, respectively, as shown in Fig. 2(b). As a result, the total energy of the system is lowered by 124.97 meV from that of the spin-unpolarized state.

Similarly, as shown in Fig. 6(b), in 6ZBNNR-N-(6,6)SWCNT, there two partial-filled bands, marked with $H\Gamma-0$ and $H\Gamma-1$, or $LX+0$ and $HX-0$, crossing the Fermi level. Clearly, the partial charge densities of the unoccupied band and the occupied band plotting in Fig. 6(b) show that two partial-filled bands corresponding electron states are heavily localized. Indeed, as shown in Fig. 7(b), the LDOS analysis reveal that they are strongly localized on the C_1 and C_2 atoms of “-(6,6)SWCNT” as well as the edge-B atom of “6ZBNNR”. According to Hund’s rule, such partial filling of the localized bands drives spontaneous spin polarization, resulting in exchange splittings, shown in Fig. 2(a), between

**Fig. 8** (a) Geometric structure, band structure, and TDOS as well as the LDOS of the edge-B and edge-N atoms for 6ZBNNR. (b) Geometric structure and band structure of (6,6)SWCNT. “o” and “ Δ ” label special bands (see Fig. 6). The other marks are same as in Fig. 2.

$\downarrow L\Gamma+0$ and $\uparrow H\Gamma-0$ bands, as well as between $\downarrow L\Gamma+1$ and $\uparrow H\Gamma-1$ bands, respectively. As a result, the total energy of the system is lowered by 460.20 meV from that of the nonmagnetic state.

3.2 Stability

3.2.1 Formation energy and covalent bonds

The formation energy of the hybrid structures of ZBNNR/SWCNT, which is usually used to characterize the stability of the system structure, is defined as^{67,68}

$$E_f = E_{\text{tot}} - E_{n\text{-ZBNNR}} - E_{(m,m)\text{SWCNT}} \quad (1)$$

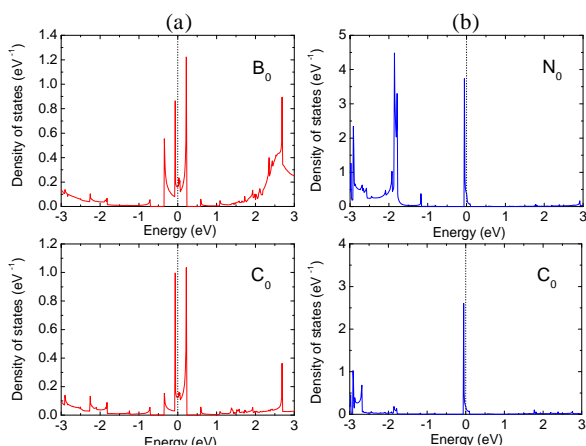
where, E_{tot} is the total energies of the system, $E_{n\text{-ZBNNR}}$ is the energy of pristine n -ZBNNR, and $E_{(m,m)\text{SWCNT}}$ is the energy of the (m,m) SWCNT. The calculated results for n ZBNNR-B-(6,6)SWNT and n ZBNNR-N-(6,6)SWNT are listed in Table 5. The negative formation energy for all systems found in this work indicates that all hybrid structures of ZBNNR/SWCNT not only are steady, but also can be spontaneously formed. Moreover, one can notice that n ZBNNR-B-(6,6)SWNT is more stable than n ZBNNR-N-(6,6)SWNT, such as the formation energy of 6ZBNNR-B-(6,6)SWNT is -2.56 eV, whereas the formation energy of 6ZBNNR-N-(6,6)SWNT is -2.18 eV. In order to explore the binding nature of the n -ZBNNR and (6,6)SWNT interaction, as shown in Fig. 8, we plot the band structure, TDOS and the LDOS (edge-B and edge-N atoms) of 6-ZBNNR, as well as band the structure of (6,6)SWCNT. As show in Fig. 8(a), near Fermi level of 6-ZBNNR, there are four energy bands. TDOS and LDOS analysis reveal that the energy bands marked with “ Δ ” mainly originate from the 2p orbitals of the edge-B atoms, whereas the energy bands

Table 6 The Mulliken charge on specific atoms in 6ZBNNR, (6,6)SWCNT, 6ZBNNR-B-(6,6)SWCNT and 6ZBNNR-N-(6,6)SWCNT.

Atoms	edge-B(B_0)	edge-N(N_0)	C_0	C_1	C_2
6ZBNNR	2.766	5.275			
(6,6)SWCNT			4.000	4.000	4.000
6ZBNNR-B-(6,6)SWCNT	2.754	5.295	4.014	3.848	4.033
6ZBNNR-N-(6,6)SWCNT	2.807	5.559	3.719	3.946	4.008

Table 7 The hydrogen adsorption energy per edge atom in the unit of eV for H- n ZBNNR-B-(6,6)SWNT and H- n ZBNNR-N-(6,6)SWNT.

System	$n=3$	$n=4$	$n=5$	$n=6$	$n=7$	$n=8$
H- n ZBNNR-B-(6,6)SWNT	-2.95	-2.98	-2.84	-2.80	-2.79	-2.79
H- n ZBNNR-N-(6,6)SWNT	-2.80	-2.80	-2.80	-2.81	-2.80	-2.80

**Fig. 9** (a) LDOS of the B_0 and C_0 atoms for 6ZBNNR-B-(6,6)SWCNT. (b) LDOS of the N_0 and C_0 atoms for 6ZBNNR-N-(6,6)SWCNT. The other marks are same as in Fig. 2.

marked with "o" mainly originate from the 2p orbitals of the edge-N atoms. On the other hand, as shown in Fig. 8(b), near Fermi level of (6,6)SWCNT, two energy bands originate from the 2p orbitals of the C atoms. After 6-ZBNNR bonding with (6,6)SWCNT via edge-B atoms, as shown in Fig. 6(a), the energy bands marked with "o" remain almost unchanged. However, the energy bands marked with " Δ " disappear, owing to the 2p orbitals of the edge-B atoms to strongly couple with the 2p orbitals of the C atoms forming a covalent band labeled as LI^+0 and $HX-0$ in Fig. 6(a), namely the B_0 - C_0 band in 6ZBNNR-B-(6,6)SWNT is the covalent band. In contrast, after 6-ZBNNR bonding with (6,6)SWCNT via edge-N atoms, as shown in Fig. 6(b), the energy bands marked with " Δ " remain almost unchanged. Whereas, the energy bands marked with "o" disappear, due to the 2p orbitals of the edge-N atoms to strongly couple with the 2p orbitals of the C atoms forming a covalent band labeled as HI^-0 and $HX-0$ in Fig. 6(b), namely the N_0 - C_0 band in 6ZBNNR-N-(6,6)SWNT belong to a covalent band.

In order to gain further insight into the B_0 - C_0 band and the N_0 - C_0 band, LDOS of the B_0 and C_0 atoms for 6ZBNNR-B-(6,6)SWCNT, as well as LDOS of the N_0 and C_0 atoms for 6ZBNNR-N-(6,6)SWCNT, are plotted in Fig. 9. From Fig. 9(a), one can find that the strong hybridization of B_0 and C_0 states demonstrates the formation of covalent bonds. Similarly, as shown in Fig. 9(b), the strong hybridization of N_0 and C_0 states

demonstrates the formation of covalent bonds. However, the formation energy difference between 6ZBNNR-B-(6,6)SWNT and 6ZBNNR-N-(6,6)SWNT originates from the electronegativity of the N, C, and B atoms. It is known that electronegativity is the intrinsic property measuring the escaping tendency of electrons from atomic species. The larger the value of the electronegativity, the greater the atom's strength to attract a bonding pair of electrons. The electronegativity values for N, C, and B atoms are 3.04, 2.55, and 2.04, respectively. We note that the electronegativity difference of the N and C atoms (1.49) is larger than that of the C and B atoms (0.51). Thus, the N_0 - C_0 band in 6ZBNNR-N-(6,6)SWNT approaches to ionic bond, which can be demonstrated by the Mulliken charge analysis before and after 6-ZBNNR bonding with (6,6)SWCNT. As listed in Table 6, before 6-ZBNNR bonding with (6,6)SWCNT, the Mulliken charge analysis shows the charge of 2.766, 5.275, and 4.000 e on each edge-B, edge-N, and C_0 atom, respectively. After 6-ZBNNR bonding with (6,6)SWCNT via edge-B atoms, the Mulliken charge analysis shows the charge of 2.754, 5.295, and 4.014 e on each B_0 , edge-N atom, and C_0 , respectively, namely there is no obvious transfer of electron from the B_0 atoms to the C_0 atoms. However, after 6-ZBNNR bonding with (6,6)SWCNT via edge-N atoms, the Mulliken charge analysis shows the charge of 2.807, 5.559, and 3.719 e on each edge-B, N_0 , and C_0 atom, respectively, namely there is obvious transfer of electron from the C_0 atoms to the N_0 atoms, showing that the N_0 - C_0 band in 6ZBNNR-N-(6,6)SWNT approaches to ionic bond. As a result, n ZBNNR-B-(6,6)SWNT is more stable than n ZBNNR-N-(6,6)SWNT.

3.2.2 Hydrogen adsorption energy

On the other hand, the hydrogen adsorption energy per edge atom, which quantifies the gain in energy of a hydrogenation of hybrid structures of ZBNNR/SWCNT as compared to a pristine system and molecular hydrogen, is given by⁶⁸

$$E_{\text{ads}}^{\text{H}} = (E_{\text{tot}} - E_{\text{pristine}} - n_{\text{H}} \frac{E_{\text{H}_2}}{2}) / N_{\text{edge}} \quad (2)$$

where, E_{tot} is the total energies of the hydrogenation system where the dangling bonds associated with edge C atoms are saturated with single H atoms and n_{H} is the total number of such H atoms. E_{H_2} is the energy of the hydrogen molecule and the factor of 2 in the last term accounts for the fact that each H_2 molecule only contributes one H atom to each initially unsaturated bond. E_{pristine} is the total energies of the pris-

tine system, whereas, N_{edge} is the number of edge C atoms per unit cell. The calculated results for $n\text{ZBNNR-B-(6,6)SWNT}$ and $n\text{ZBNNR-N-(6,6)SWNT}$ are listed in Table 7. We note that the negative hydrogen adsorption energy for all hybrid structures of ZBNNR/SWCNT are found in this work, which indicates that hydrogenation leads to an increase of binding energy, namely the hydrogen adsorption is favored.

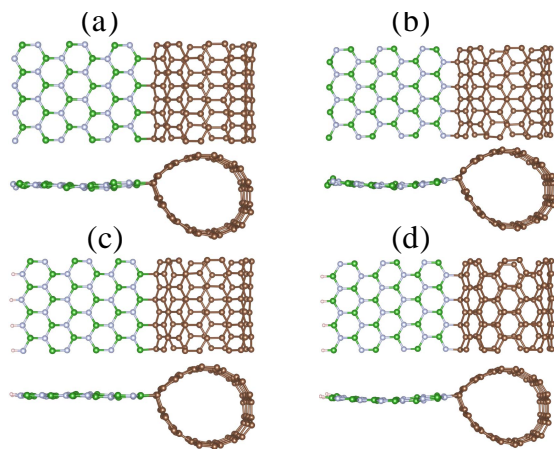


Fig. 10 At the simulation time 6.0 ps, top view and side view of snapshots. (a) 6ZBNNR-B-(6,6)SWCNT. (b) 6ZBNNR-N-(6,6)SWCNT. (c) H-6ZBNNR-B-(6,6)SWCNT. (d) H-6ZBNNR-N-(6,6)SWCNT. The other marks are same as in Fig. 1 and Fig. 3.

3.2.3 ab initio MD simulations

In order to further examine whether hybrid structures of ZBNNR/SWCNT are stable at room temperature, ab initio MD simulations are performed. For example, at the simulation time 6.0 ps, the snapshots of structures of the 6ZBNNR-B-(6,6)SWNT, 6ZBNNR-N-(6,6)SWNT, H-6ZBNNR-B-(6,6)SWNT, and H-6ZBNNR-N-(6,6)SWNT are shown in Fig. 10. Clearly, although a small distortion is found at B-edge or N-edge, the essential structures of the 6ZBNNR-B-(6,6)SWNT, 6ZBNNR-N-(6,6)SWNT, H-6ZBNNR-B-(6,6)SWNT, and H-6ZBNNR-N-(6,6)SWNT, are intact, namely they are quite stable at room temperature. This is ascribable to its sp^3 -hybridized Y-shape and remaining tube-shape stability structures commonly used for building construction. On the other hand, comparing between Fig. 10(a) and Fig. 10(c), as well as Fig. 10(b) and Fig. 10(d), one can find that the distortion of the hydrogenation edge is less than that of the pristine edge, owing to H-passivation releasing the edge energy.

3.2.4 Fully spin polarized controlling by carrier doping

It is known that the Fermi level can be shifted up and down by altering the sign of the gate voltages (the well-known field-effect transistor (FET) doping technique). Therefore, in order to demonstrate that in 2ZBNNR-N-(6,6)SWCNT FET not only the excited electrons but also the holes can be fully spin polarized,⁵¹ we calculate the TDOS of 2ZBNNR-N-(6,6)SWCNT with x electrons added or removed per unit cell ($x < 0$ for electron doping, $x = 0$ for undoping, and $x > 0$ for hole doping). As shown in Fig. 11(b), when $x = 0.0$, both the electron and hole spins

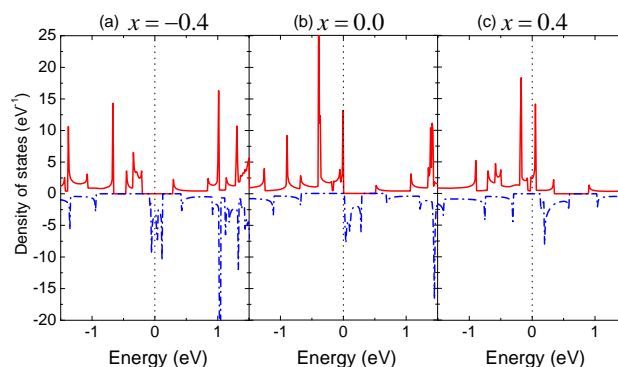


Fig. 11 TDOS of 2ZBNNR-N-(6,6)SWCNT with x electrons added or removed per unit cell ($x < 0$ for electron doping, $x = 0$ for undoping, and $x > 0$ for hole doping). The other marks are same as in Fig. 2.

are not spin polarized. However, as shown in Fig. 11(a), when $x = -0.4$ (electron doping), the electrons are fully spin polarized. In contrast, as shown in Fig. 11(c), when $x = 0.4$ (hole doping), the holes are fully spin polarized. Clearly, such novel phenomenon is originated from the unique band structures of $n\text{ZBNNR-N-(}m,m\text{)SWCNTs}$. In order to check the unique band structures of $n\text{ZBNNR-N-(}m,m\text{)SWCNTs}$, additional ab initio Heyd-Scuseria-Ernzerh screened hybrid functional (HSE06⁶⁹) calculation has been carried out using the Quantum-ESPRESSO package.⁷⁰ The result shows that the unique band structure is robust with respect to the different treatments of electronic exchange and correlation even though the different treatments of electronic exchange and correlation lead to the quantitative difference in band structure (ESI Fig. 1†).

4 Conclusions

In summary, we have studied the hybrid structures of ZBNNR/SWCNT by using standard spin-polarized density functional theory calculations as well as ab initio molecular dynamics simulations. Several important results are summarized as follows:

1. All examined hybrid structures are stable at room temperature.
2. The structure of ZBNNR-B-SWCNT is more stable than that of ZBNNR-N-SWCNT.
3. ZBNNR-B-SWCNT belongs to the intrinsic ferromagnetic metal.
4. ZBNNR-N-SWCNT belongs to the ferromagnetic intrinsic SGS.
5. In the H-ZBNNR-B-SWCNT, hydrogenation removes the dangling-bond states at its N-edge, whereas the electrically conductive function and magnetic properties of "–SWCNT" edge remain unchanged. However, in the H-ZBNNR-N-SWCNT, hydrogenation removes the dangling-bond states at its B-edge, but only the magnetic properties of "–SWCNT" edge remain unchanged.
6. Hydrogenation induces a SGS-spin-semiconductor transition in the H-ZBNNR-N-SWCNT.

Acknowledgement

This work was supported by the National Natural Science Foundation of China (grant no. 11174003) and the 211 Project of Anhui University.

References

- 1 Y. -W. Son, M. L. Cohen and S. G. Louie, *Phys. Rev. Lett.*, 2006, **97**, 216803.
- 2 Y. -W. Son, M. L. Cohen and S. G. Louie, *Nature* (London), 2006, **444**, 347-349.
- 3 W. Y. Kim, K. S. Kim, *Nature Nanotech.*, 2008, **3**, 408-412.
- 4 T. B. Martins, A. J. R. da Silva and R. H. Miwa, *Nano Lett.*, 2008, **8**, 2293-2298.
- 5 B. Mandal, . Sarkar, A. Pramanika and P. Sarkar, *RSC Adv.*, 2014, **4**, 49946-49952.
- 6 D. Yu, E. M. Lupton, M. Liu, W. Liu and F. Liu, *Nano Res.*, 2008, **1**, 56-62.
- 7 D. Yu, E. M. Lupton, H. J. Gao, C. Zhang and F. Liu, *Nano Res.*, 2008, **1**, 497-501.
- 8 D. -E. Jiang, B. G. Sumpter and Sheng. Dai, *J. Phys. Chem. B*, 2006, **110**, 23628-23632.
- 9 D. -E. Jiang, B. G. Sumpter and Sheng. Dai, *J. Chem. Phys.*, 2007, **126**, 134701.
- 10 J.-I. Takashiro, Y. Kudo, S.-J. Hao, K. Takai, D. N. Futaba, T. Enoki and M. Kiguchi, *Phys. Chem. Chem. Phys.*, 2014, **16**, 21363-21371.
- 11 O. Hod, V. Barone, J. E. Peralta and G. E. Scuseria, *Nano Lett.*, 2007, **7**, 2295-2299.
- 12 E. -J. Kan, Z. Li, J. -L. Yang and J. G. Hou, *J. Am. Chem. Soc.*, 2008, **130**, 4224-4225.
- 13 M. H. Wu, X. J. Wu and X. C. Zeng, *J. Phys. Chem. C*, 2010, **114**, 3937-3944.
- 14 D. Gunlycke, J. Li, J. W. Mintmire and C. T. White, *Appl. Phys. Lett.*, 2007, **91**, 112108.
- 15 M. H. Wu, Y. Pei and X. C. Zeng, *J. Am. Chem. Soc.*, 2010, **132**, 5554-5555.
- 16 Y. Zou, M. Long, M. Li, X. Zhang, Q. Zhang and H. Xu, *RSC Adv.*, 2015, **5**, 19152-19158
- 17 V. Barone and J. E. Peralta, *Nano Lett.*, 2008, **8**, 2210-2214.
- 18 M. Terrones, J. C. Charlier, A. Gloter, E. Cruz-Silva, E. Terres, Y. B. Li, Z. Zanolli, J. M. Dominguez, H. Terrones, Y. Bando and D. Golberg, *Nano Lett.*, 2008, **8**, 1026-1032.
- 19 F. Zheng, G. Zhou, Z. Liu, J. Wu, W. Duan, B. Gu and S. B. Zhang, *Phys. Rev. B*, 2008, **78**, 205415.
- 20 L. Lai, J. Lu, L. Wang, G. F. Luo, J. Zhou, R. Qin, Z. X. Gao and W. N. Mei, *J. Phys. Chem. C*, 2009, **113**, 2273-2276.
- 21 E. Kan, F. Wu, H. Xiang, J. Yang and M. -H. Whangbo, *J. Phys. Chem. C*, 2011, **115**, 17252-17254.
- 22 Z. H. Zhang and W. L. Guo, *Phys. Rev. B*, 2008, **77**, 075403.
- 23 M. Topsakal, E. Akturk and S. Ciraci, *Phys. Rev. B*, 2009, **79**, 115442.
- 24 R. Mukherjee and S. Bhowmick, *J. Chem. Theory Comput.*, 2011, **7**, 720-724.
- 25 Y. Wang, Y. Li and Z. Chen, *J. Phys. Chem. C*, 2014, **118**, 25051-25056.
- 26 D. Krepel and O. Hod, *J. Chem. Theory Comput.*, 2014, **10**, 373-380.
- 27 A. Lopez-Bezanilla, J. Huang, H. Terrones and B. G. Sumpter, *J. Phys. Chem. C*, 2012, **116**, 15675-15681.
- 28 A. Lopez-Bezanilla, J. Huang, H. Terrones and B. G. Sumpter, *Nano Lett.*, 2011, **11**, 3267-3273.
- 29 L. L. Song, X. H. Zheng, H. Hao, J. Lan, X. L. Wang and Z. Zeng, *RSC Adv.*, 2014, **4**, 48212-48219.
- 30 P. Tang, X. Zou, S. Wang, J. Wu, H. Liu and W. Duan, *RSC Adv.*, 2012, **2**, 6192-6199.
- 31 G. Yu, D. Liu, W. Chen, H. Zhang and X. Huang, *J. Phys. Chem. C*, 2014, **118**, 12880-12889.
- 32 D. Ghosh, P. Parida and S. K. Pati, *J. Phys. Chem. C*, 2014, **118**, 14670-14676.
- 33 S. Tang and S. Zhang, *J. Phys. Chem. C*, 2013, **117**, 17309-17318.
- 34 W. Chen, Y. Li, G. Yu, Z. Zhou and Z. Chen, *J. Chem. Theory Comput.*, 2009, **5**, 3088-3095.
- 35 A. Du, S. C. Smith and G. Lu, *Chem. Phys. Lett.*, 2007, **447**, 181-186.
- 36 W. Chen, Y. Li, G. Yu, C. -Z. Li, S. B. Zhang, Z. Zhou and Z. Chen, *J. Am. Chem. Soc.*, 2010, **132**, 1699-1705.
- 37 J. Qi, X. Qian, L. Qi, Q. Feng, D. Shi and J. Li, *Nano Lett.*, 2012, **12**, 1224-1208.
- 38 C.-H. Park and S. G. Louie, *Nano Lett.*, 2008, **8**, 2200-2203.
- 39 R. S. Krsmanović and Z. Šljivančanin, *J. Phys. Chem. C*, 2014, **118**, 16104-16112.
- 40 J. He, K. Q. Chen, Z. Q. Fan, L. M. Tang and W. P. Hu, *Appl. Phys. Lett.*, 2010, **97**, 193305.
- 41 Z. Yu, M. L. Hu, C. X. Zhang, C. Y. He, L. Z. Sun and J. Zhong, *J. Phys. Chem. C*, 2011, **115**, 10836-10841.
- 42 Y. Liu, X. Wu, Y. Zhao, X. C. Zeng and J. Yang, *J. Phys. Chem. C*, 2011, **115**, 9442-9450.
- 43 J. Yu and W. Guo, *J. Phys. Chem. Lett.*, 2013, **4**, 951-955.
- 44 Y. Wang, Y. Ding and J. Ni, *J. Phys. Chem. C*, 2012, **116**, 5995-6003.
- 45 C. Tang, L. Kou and C. Chen, *Chem. Phys. Lett.*, 2012, **523**, 98-103.
- 46 S. Dutta, A. Manna and S. Pati, *Phys. Rev. Lett.*, 2009, **102**, 096601.
- 47 S. Tang and Z. Cao, *Phys. Chem. Chem. Phys.*, 2010, **12**, 2313-2320.
- 48 A. Du, Y. Chen, Z. Zhu, G. Lu and S. C. Smith, *J. Am. Chem. Soc.*, 2009, **131**, 1682-1683.
- 49 A. Du, S. Sanvito and S. C. Smith, *Phys. Rev. Lett.*, 2012, **108**, 197207.
- 50 S. Sanvito, *Chem. Soc. Rev.*, 2011, **40**, 3336-3355.
- 51 X. Wang, *Phys. Rev. Lett.*, 2008, **100**, 156404.
- 52 S. Ouardi, G. H. Fecher, C. Felser and J. Kubler, *Phys. Rev. Lett.*, 2013, **110**, 100401.
- 53 Z. F. Wang, S. Jin and F. Liu, *Phys. Rev. Lett.*, 2013, **111**,

- 096803.
- 54 X. Chen, Y. Liu, B. -L. Gu, W. Duan and F. Liu, *Phys. Rev. B*, 2014, **90**, 121403(R).
- 55 P. Lou, *Phys. Chem. Chem. Phys.*, 2015, **17**, 7949-7959.
- 56 OpenMX Website. T. Ozaki, H. Kino, J. Yu, M. J. Han, N. Kobayashi, M. Ohfuti, F. Ishii, T. Ohwaki and H. Weng, <http://www.openmx-square.org/>.
- 57 J. P. Perdew, K. Burke and M. Ernzerhof, *Phys. Rev. Lett.*, 1996, **77**, 3865-3868.
- 58 N. Troullier and J. L. Martins, *Phys. Rev. B*, 1991, **43**, 1993-2006.
- 59 T. Ozaki, *Phys. Rev. B*, 2003, **67**, 155108.
- 60 T. Ozaki and H. Kino, *Phys. Rev. B*, 2004, **69**, 195113.
- 61 H. J. Monkhorst and J. D. Pack, *Phys. Rev. B*, 1976, **13**, 5188-5192.
- 62 P. Lou and J. Y. Lee, *J. Phys. Chem. C*, 2010, **114**, 10947-10951.
- 63 P. Lou, *J. Phys. Chem. C*, 2014, **118**, 4475-4482.
- 64 P. Lou, *J. Mater. Chem. C*, 2013, **1**, 2996-3003.
- 65 S. Nosé, *J. Chem. Phys.*, 1984, **81**, 511-519.
- 66 S. Nosé, *Mol. Phys.*, 1984, **52**, 255-268.
- 67 P. Lou, *Phys. Status Solidi RRL*, 2014, **8**, 187-190.
- 68 P. Lou, *Phys. Chem. Chem. Phys.*, 2011, **13**, 17194-17204.
- 69 J. Heyd, G. E. Scuseria and M. Ernzerhof, *J. Chem. Phys.* 2006, **124**, 219906.
- 70 P. Giannozzi, S. Baroni, N. Bonini, M. Calandra, R. Car, C. Cavazzoni, D. Ceresoli, G. L. Chiarotti, M. Cococcioni, I. Dabo, A. Dal Corso, S. Fabris, G. Fratesi, S. de Gironcoli, R. Gebauer, U. Gerstmann, C. Gougoussis, A. Kokalj, M. Lazzeri, L. Martin-Samos, N. Marzari, F. Mauri, R. Mazzarello, S. Paolini, A. Pasquarello, L. Paulatto, C. Sbraccia, S. Scandolo, G. Sciauzero, A. P. Seitsonen, A. Smogunov, P. Umari, and R. M. Wentzcovitch, *J. Phys.: Condens. Matter* 2009, **21**, 395502.